

# Novel Inhibitors of DNA Gyrase: 3D Structure Based Biased Needle Screening, Hit Validation by Biophysical Methods, and 3D Guided Optimization. A Promising Alternative to Random Screening

Hans-Joachim Boehm, Markus Boehringer,\* Daniel Bur, Hans Gmuender, Walter Huber, Werner Klaus, Dirk Kostrewa, Holger Kuehne, Thomas Luebbers, Nathalie Meunier-Keller, and Francis Mueller

Preclinical Research, Pharmaceuticals Division, F. Hoffmann-La Roche Ltd., CH-4070 Basel, Switzerland

Received January 18, 2000

Random screening provided no suitable lead structures in a search for novel inhibitors of the bacterial enzyme DNA gyrase. Therefore, an alternative approach had to be developed. Relying on the detailed 3D structural information of the targeted ATP binding site, our approach combines as key techniques (1) an in silico screening for potential low molecular weight inhibitors, (2) a biased high throughput DNA gyrase screen, (3) validation of the screening hits by biophysical methods, and (4) a 3D guided optimization process. When the in silico screening was performed, the initial data set containing 350 000 compounds could be reduced to 3000 molecules. Testing these 3000 selected compounds in the DNA gyrase assay provided 150 hits clustered in 14 classes. Seven classes could be validated as true, novel DNA gyrase inhibitors that act by binding to the ATP binding site located on subunit B: phenols, 2-amino-triazines, 4-amino-pyrimidines, 2-amino-pyrimidines, pyrrolopyrimidines, indazoles, and 2-hydroxymethyl-indoles. The 3D guided optimization provided highly potent DNA gyrase inhibitors, e.g., the 3,4-disubstituted indazole **23** being a 10 times more potent DNA gyrase inhibitor than novobiocin (**3**).

## Introduction

The identification of an appropriate lead structure is a vital step for any pharmaceutical research project. Usually, lead structures are identified by random screening of hundreds of thousands of compounds. However, in some cases no suitable leads are found by this approach. Without lead structures research projects usually have to be discontinued even if they aim to cover urgent medical needs with outstanding market potentials.

Seeking novel inhibitors of DNA gyrase (E.C. 5.99.1.3), we have been facing a similar situation. DNA gyrase is a well-established antibacterial target.<sup>1,2</sup> It is an essential, prokaryotic type II topoisomerase with no direct mammalian counterpart. It is involved in the vital processes of DNA replication, transcription, and recombination. DNA gyrase catalyzes the ATP-dependent introduction of negative supercoils into bacterial DNA as well as the decatenation and unknotting of DNA. The enzyme consists of two subunits, A and B, of molecular mass 97 and 90 kDa, respectively, with the active enzyme being an A<sub>2</sub>B<sub>2</sub> complex. The A subunit of DNA gyrase is involved in DNA breakage and reunion while the B subunit catalyzes the hydrolysis of ATP. DNA gyrase is inhibited by quinolones, coumarins, and cyclothialidines (Figure 1), which, however, all have their own limitations. Quinolones, e.g., ciprofloxacin (**1**), which inhibit the DNA breakage–reunion cycle by binding to the subunit A and by blocking the gyrase–DNA complex, are successfully used as broad spectrum

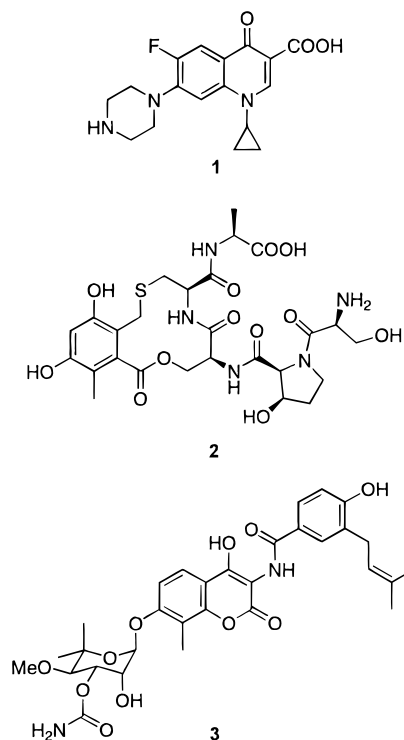


**Figure 1.** Known inhibitors of DNA gyrase: ciprofloxacin (**1**), cyclothialidine Ro 09-1437/000 (**2**), and novobiocin (**3**).

antibiotics in the clinic. Unfortunately, resistance to quinolones has already emerged,<sup>3,4</sup> and the fear of juvenile arthropathy prevents their use in pediatrics.<sup>5</sup> The two other known classes of DNA gyrase inhibitors, cyclothialidines,<sup>6</sup> e.g., Ro 09-1437/000 (**2**), and coumarins, e.g., novobiocin (**3**), bind to the ATP recognition

\* Address correspondence to Markus Boehringer, F. Hoffmann-La Roche Ltd., Pharmaceuticals Division, Preclinical Research, PRBC, Bldg. 15/136, CH-4070 Basel, Switzerland. Tel: ++41 61 688 8507. Fax: ++41 61 688 6459. E-mail: markus.boehringer@roche.com.

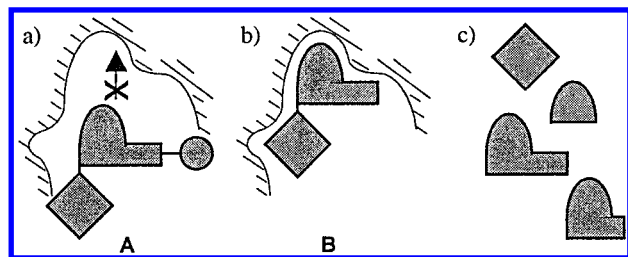


**Figure 2.** (a) Compound A cannot bind to the active site due to steric interference of an inappropriate side chain. (b) Compound B lacking the inappropriate side chain can bind to the active site. (c) Four needle type compounds.

site located in the subunit B.<sup>7,8</sup> This target site may offer advantages such as a lack of cross-resistance with quinolones. Novobiocin (**3**) was clinically used against *Staphylococcus aureus*, including multi-resistant *S. aureus* (MRSA). However, it suffers from toxicity and a rapidly developing resistance.<sup>9,10</sup> As demonstrated by the cyclothialidines, this type of resistance can be overcome.<sup>11</sup> The limitations of the cyclothialidines are their insufficient in vivo activities due to a class specific rapid and extensive glucuronidation of the essential phenol moiety.<sup>12</sup>

To overcome the limitations of the known DNA gyrase inhibitors, we have been searching for novel structures. However, beside the known inhibitors, quinolones, coumarins, and cyclothialidines, random screening has not provided other suitable hits. Therefore, we have been developing a new rational approach to generate lead structures by using the detailed 3D structural information of the ATP binding site located on subunit B. This approach combines as key techniques (1) an in silico screen for potential low molecular weight inhibitors, (2) a robust and sensitive biased high throughput DNA gyrase screen based on the results of the in silico screen, (3) validation of the screening hits relying mainly on biophysical methods, and (4) a 3D guided optimization process.

### Concept of Needle Screening

There are definitely various reasons why a compound could be inactive in an enzyme assay. A sterically or electronically inappropriate side chain, for example, might be the reason for converting an active core structure into an inactive compound (Figure 2). As a consequence of such considerations we became interested in screening for low molecular weight inhibitors, i.e., for inhibitors that are reduced to the minimal structural elements while still fitting perfectly into the active site and fulfilling the essential binding requirements to exhibit a maximal biological effect. We call these low molecular weight inhibitors (MW < 300) *needles* since they should be able to penetrate into deep and narrow channels and subpockets of active sites like a fine, sharp needle probing the surface of an active site (Figure 2).

The attractiveness of the needle screening lies in the small and compact structure of the needle: (1) The needle is devoid of any unnecessary structural elements that, for example, might result in toxicity or metabolic instability. (2) A later introduction of tailored side chains during a following optimization process does not per se lead to oversized molecules having, e.g., bio-

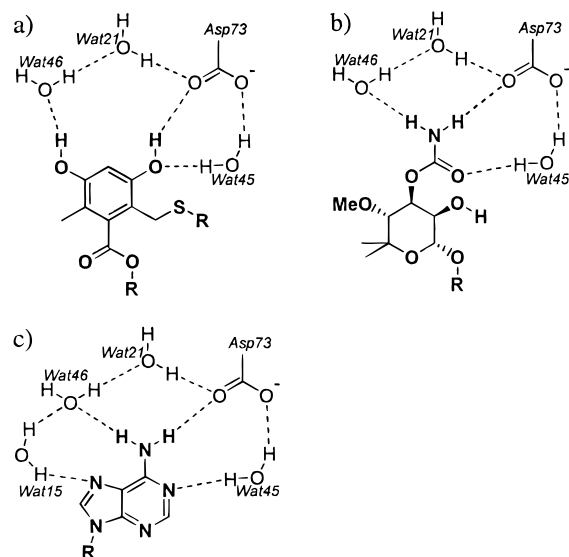


**Figure 3.** The common hydrogen bond network between three different ligands and DNA gyrase, including critical water molecules (Wat), determined by X-ray analysis. (a) The phenolic moiety of cyclothialidine forms hydrogen bonds with Asp73, Wat45, and Wat46. SAR of cyclothialidine derivatives revealed that the hydroxyl group hydrogen bonding to Wat46 can be replaced, e.g., by MeO, with gain in binding affinity, indicating that this H-bond is not essential. (b) Hydrogen bonds formed by the carbamate moiety of novobiocin in the DNA gyrase binding pocket. (c) Hydrogen bonds between the adenine part of ADPNP and the DNA gyrase binding pocket.

availability problems. (3) The needle and its derivatives are most likely structures relatively easy and inexpensive to be synthesized compared to complex natural products.

### In Silico Needle Screening

Beside profound SAR for inhibition of DNA gyrase by cyclothialidine derivatives,<sup>13,14</sup> detailed three-dimensional structural information was available about the ATP binding site of DNA gyrase from the Gram negative *Escherichia coli* as well as from the Gram positive *S. aureus*. At that time we had access to the X-ray structures of the N-terminal 43 kDa or 24 kDa fragment, respectively, of subunit B of DNA gyrase from *E. coli* complexed with the substrate analogue ADPNP<sup>8</sup> as well as complexed with the two structurally different inhibitors cyclothialidine **2** and novobiocin (**3**).<sup>7</sup> Although these ligands bind to the same enzyme pocket, they occupy common as well as very different subregions. In the inner part of the pocket they all share a common binding motive: each of them donates a hydrogen bond to an aspartic acid side chain (Asp73)<sup>15</sup> and accepts a hydrogen bond from a conserved water molecule (Wat45) (Figure 3). We reasoned that a novel inhibitor should have the ability to form these two key hydrogen bonds. In addition, it should contain a lipophilic part satisfying the steric and lipophilic requirements of the enzyme pocket. This pharmacophore hypothesis is schematically summarized in Figure 4.

A 3D database screening was performed to identify molecules that could fulfill our pharmacophore hypothesis. The programs LUDI<sup>16,17</sup> and CATALYST<sup>18</sup> were employed to search the Available Chemicals Directory (ACD) and a part of the Roche compound inventory (RCI), i.e., a combined data set that contained about

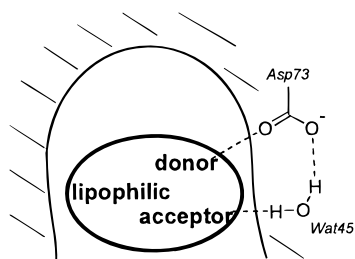


**Figure 4.** Initial binding hypothesis used for in silico screening by LUDI and Catalyst.

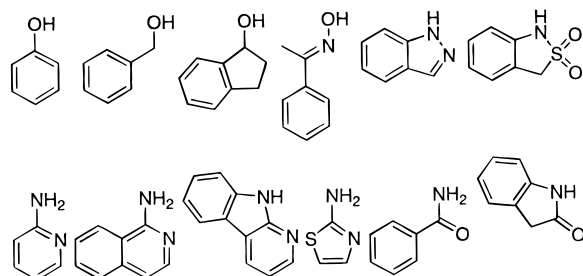


**Figure 5.** Typical needle structures obtained from the LUDI search.

350 000 compounds. LUDI was used to dock small needle type molecules into the binding site. The 3D structures of needles were generated by the computer program CORINA.<sup>19</sup> Only those molecules were accepted as valid hits that in silico form both critical hydrogen bonds. Typical needle structures obtained from the LUDI search are shown in Figure 5. Not only these depicted unsubstituted needles were selected but also appropriately substituted analogues with a MW < 300. The LUDI search resulted in a list of about 200 molecules that were tested for their DNA gyrase inhibitory activity. The CATALYST search required the precise topological definition of essential ligand enzyme interactions, i.e., *H-bond donors/acceptors*, *van der Waals interactions*, and *excluded volumes*. The precise positions and types of these key interactions were defined in the cyclothialidine–DNA gyrase X-ray structure using our molecular modeling program MOLOC.<sup>20</sup> An RCI subdatabase containing multiple conformations of each molecular entity was searched. Molecules with a molecular weight of >400 were excluded. Clustering using Tanimoto as implemented in the Daylight system<sup>21</sup> and manual selection of representatives led to a total of 400 potential DNA gyrase inhibitors. In addition, several closely related analogues of the hits from the two 3D database searches were included in the list of compounds to be tested.

Furthermore, kinase inhibitors known from literature were docked into the binding site of DNA gyrase. Promising structures, i.e., those that might be able to fulfill the pharmacophore hypothesis, were included in the DNA gyrase assay.

### Biased Needle Screening for DNA Gyrase Inhibitors

Only weak DNA gyrase inhibitors were expected to be found among the hits from in silico needle screening, since most of them have already been tested in the random screening performed a few years ago leading to the discovery of cyclothialidine only. Consequently,

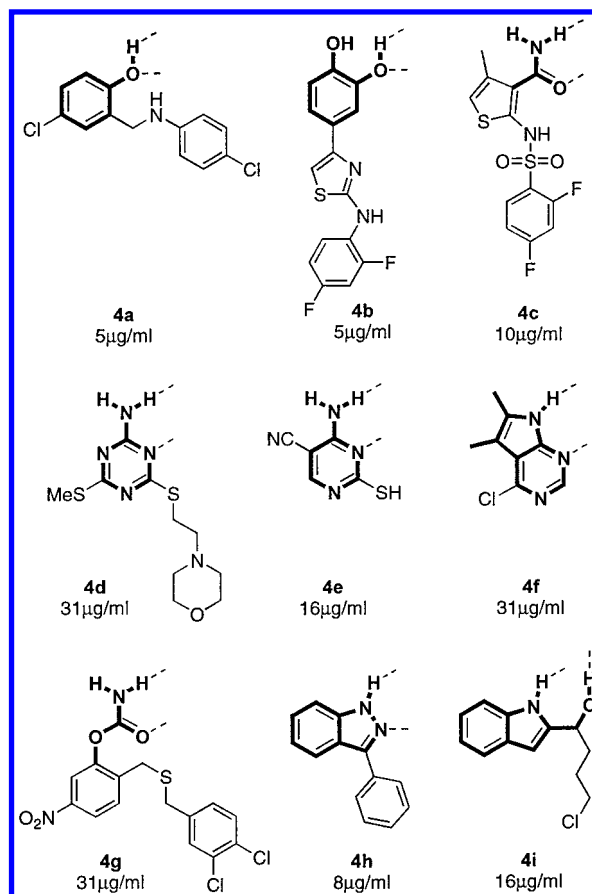


**Figure 6.** Selected hits of the biased needle screening and their *maximal noneffective concentration* (MNEC) determined in the supercoiling assay. Bold: proposed needle. Dashed bonds: postulated H-bonds to Asp73 and water Wat45. In the case of the hydroxymethyl-indole **4i** it was assumed that the hydroxymethyl group displaces Wat45.

the assay was set up in a way that allowed detecting not only highly potent but also weak inhibitors, i.e., that allowed testing compounds even in high concentrations. Instead of a supercoiling assay<sup>22</sup> usually used to test DNA gyrase inhibitory activity and used to run the above-mentioned random screening, a coupled, spectrophotometric ATPase assay<sup>23</sup> was employed containing the enzymes DNA gyrase, pyruvate kinase, and lactate dehydrogenase. Due to a higher tolerance of DMSO in the ATPase assay ( $\leq 2.5\%$ ; maximal DMSO concentration in the supercoiling assay: 0.3%) compounds could be assayed in concentrations up to 0.5 mM. ATP hydrolysis was determined monitoring the disappearance of NADH. The assay was run in the 96 well plate format.

Relying on the results of the in silico screening, just 600 compounds were tested initially. Then, close analogues of the first hits were assayed too. Overall, 3000 compounds were screened in the biased needle screen providing 150 hits. Most of them clustered in 14 classes. As expected, all hits were only weak inhibitors of DNA gyrase. Their *maximal noneffective concentration* (MNEC) was in the range of 5–64  $\mu\text{g/mL}$ , i.e., 2 to 3 orders of magnitude higher than the MNEC of novobiocin (**3**; MNEC = 0.25  $\mu\text{g/mL}$ ) or cyclothialidine (**2**; MNEC = 0.05  $\mu\text{g/mL}$ ). Representative hits are depicted in Figure 6.



## Hit Validation

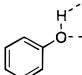
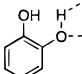
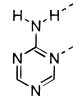
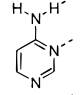
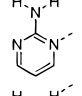
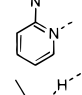
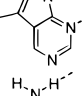
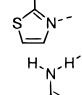
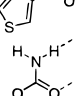
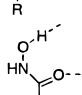
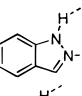
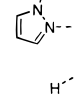
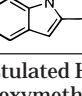
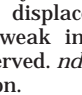
A strong emphasis was put on early validation of the screening hits and elimination of false positives due to the following considerations: (1) The hit list of any screening contains most likely a number of false positives. False positives may arise because of various reasons, e.g., unspecific binding or induction of unspecific protein aggregation. (2) Our screening assay was a coupled assay. Thus, a hit was not per se a DNA gyrase inhibitor. (3) In our search for novel inhibitors of DNA gyrase, we were focusing on compounds that act by binding to the ATP binding pocket located on subunit B. However, neither the used ATPase assay nor the supercoiling assay distinguished between compounds interfering specifically with the ATP binding site and others.

Our hit validation protocol consisted of (1) a supercoiling assay, (2) elaboration of an initial SAR with respect to the 3D structure of the active site, (3) analytical ultracentrifugation experiments, (4) surface plasmon resonance binding studies, (5) heteronuclear  $^1\text{H}/^{15}\text{N}$  correlation NMR spectroscopy, and (6) X-ray analysis.

All ATPase hits, i.e., compounds with a MNEC  $\leq 64$   $\mu\text{g}/\text{mL}$ , were subjected to the supercoiling assay in order to identify and eliminate those compounds from the hit list that acted in the ATPase assay by interfering with pyruvate kinase or lactate dehydrogenase. DNA gyrase inhibition (i.e., MNEC  $\leq 32$   $\mu\text{g}/\text{mL}$ ) was observed for compounds of all classes except for pyrazoles, hydroxamic acids, and 2-aminothiazoles (Table 1). Using the 3D structure of the ATP binding site, preliminary SARs were elaborated based on supercoiling data of the initially screened compounds as well as of some newly synthesized analogues. A *flat* SAR (i.e., no change in biological activity despite large changes in chemical structure), as, for example, observed in the case of catechols, was interpreted as a first indication of unspecific binding. The question of specific binding was addressed in more detail by several biophysical binding studies. In all these binding studies the 24 kDa N-terminal fragment of DNA gyrase subunit B of *S. aureus*<sup>41</sup> which comprised the ATP binding site was used as a model of the whole subunit B and as a model of the active DNA gyrase, i.e., the A<sub>2</sub>B<sub>2</sub> tetramer.

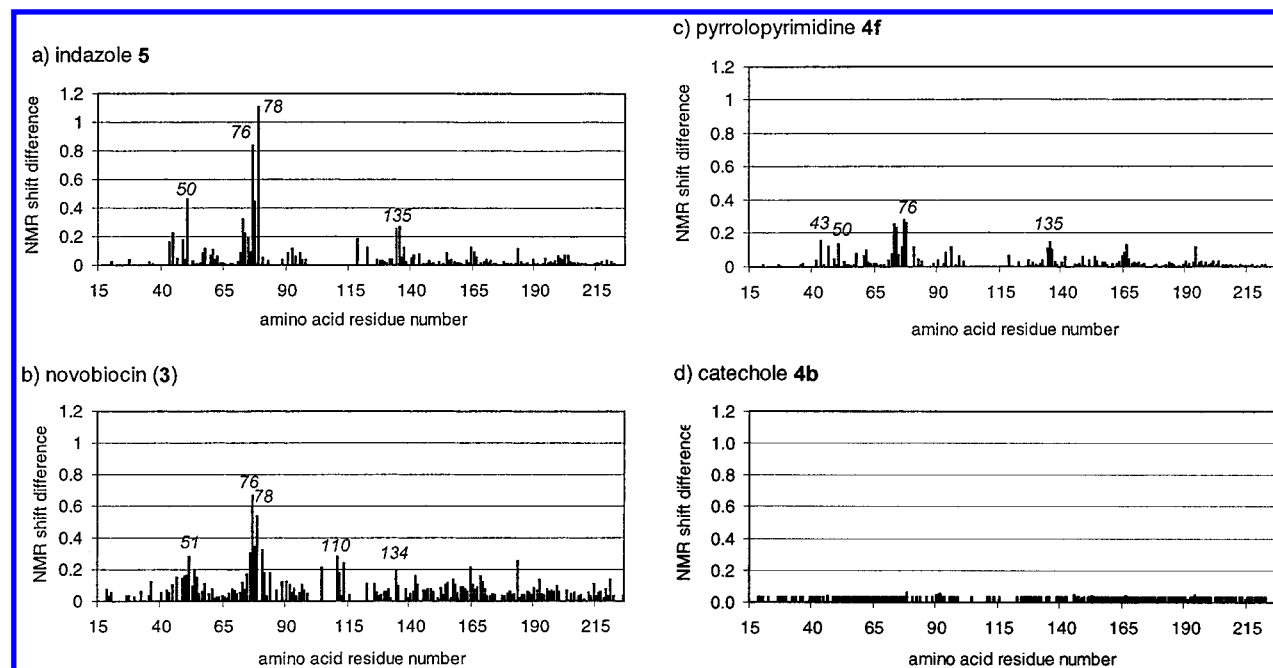
**Binding Studies by Analytical Ultracentrifugation (AUC) and Surface Plasmon Resonance (SPR).** AUC and SPR were both used as high throughput methods to identify compounds that bound to the 24 kDa fragment. Since the ATP binding pocket is located on the 24 kDa fragment, only those compounds that bound to this fragment could potentially bind to the ATP pocket. In the case of AUC, binding was detected in a sedimentation equilibrium experiment, i.e., the sample was centrifuged at the velocity required for the sedimentation–diffusion equilibrium of the 24 kDa fragment. In a typical experiment, compounds were tested at 100  $\mu\text{M}$  in the presence of 10  $\mu\text{M}$  protein. At equilibrium, the concentration profile of the potential ligand was determined by absorption measurement at different points in the sample cell. Binding of the small ligand to the heavier 24 kDa fragment results in a characteristic concentration profile.

**Table 1.** Fourteen Needle Classes of ATPase Assay Hits, Their Validation by Supercoiling Assay (SC), Analytical Ultracentrifugation (AUC), Surface Plasmon Resonance (SPR), NMR Spectroscopy (NMR), and X-ray Analysis (XR), and Their Selection for Further Optimization (SEL)<sup>a</sup>

Needles		SC	AUC	SPR	NMR	XR	SEL
phenoles		+	+	+	+	+	X
catecholes		+	nd	nd	-	nd	
2-NH <sub>2</sub> -triazines		+	+	+	+	+	X
4-NH <sub>2</sub> -pyrimidines		+	+	+	+	nd	X
2-NH <sub>2</sub> -pyrimidines		+	+	+	+	nd	X
2-NH <sub>2</sub> -pyridines		+	-	-	(+)	nd	
pyrrolopyrimidines		+	+	+	+	+	X
2-aminothiazoles		(+)	(+)	(+)	-	nd	
thiophenyl-amides		+	-	-	-	nd	
carbamates		+	-	-	-	nd	
hydroxamic acids		-	-	-	-	-	
indazoles		+	+	+	+	+	X
pyrazoles		-	nd	nd	-	nd	
2-HOCH <sub>2</sub> -indoles		+	+	+	+	-	X

<sup>a</sup> Dashed bonds: postulated H-bonds to Asp73 and water Wat45. In the case of the hydroxymethyl-indoles it was assumed that the hydroxymethyl group displaces Wat45. +: inhibition/binding observed. (+): very weak inhibition/binding observed. -: no inhibition/binding observed. nd: not determined. X: class selected for further optimization.

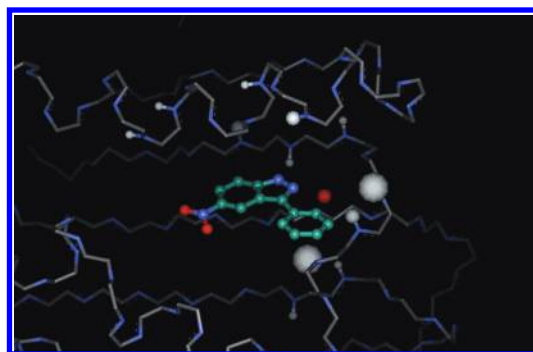
In the case of surface plasmon resonance binding experiments, the 24 kDa fragment of DNA gyrase B was immobilized on a carboxymethyl-dextran-modified gold surface in concentrations of 700–8000 pg/mm<sup>2</sup>. The compounds to be tested were exposed to these sensors in micromolar concentrations, i.e., 2.5–250  $\mu\text{M}$ . Responses that were qualitatively similar to responses for **3** were interpreted as indication of binding. Under the experimental conditions used for AUC or SPR, respec-



**Figure 7.** Shift differences of  $^1\text{H}/^{15}\text{N}$  cross-peaks of backbone amide NHs in ppm observed by heteronuclear  $^1\text{H}/^{15}\text{N}$  correlation NMR spectroscopy upon addition of potential ligands.

tively, no information on the precise site of binding could be derived. Overall, consistent results were obtained by AUC and SPR (Table 1).

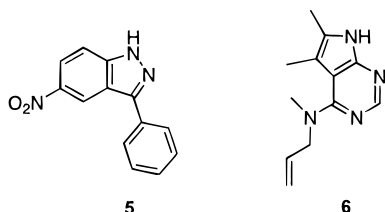
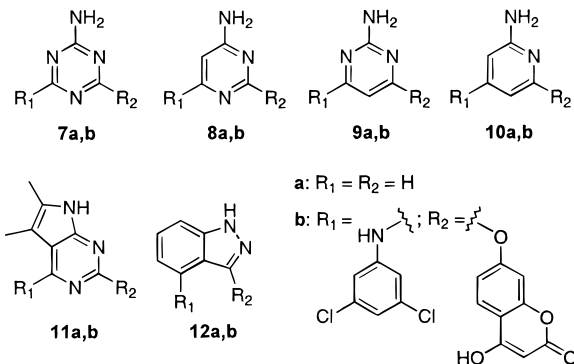
**Spin-Spin  $J$ -Coupled Heteronuclear  $^1\text{H}/^{15}\text{N}$  Correlation NMR Spectroscopy (NMR)** was used as a highly sensitive and specific method to determine if binding of a ligand to the 24 kDa fragment of DNA gyrase occurred and—more importantly—if binding occurred at the ATP binding site. This method relies on the fact that interactions of a small ligand with a protein manifest themselves in changes of the positions of resonance lines of the macromolecule.<sup>24,25</sup> The effects of binding were easily observed in the spectrum of the  $^{15}\text{N}$  isotopically labeled 24 kDa fragment. The elaborated assignment of about 80% of all NMR signals<sup>26</sup> allowed the sequence specific identification of residues with a shifted N–H signal upon binding of the ligand and subsequently the delineation of the binding epitope within the structure of the 24 kDa fragment. In the case of **5**, the most pronounced shift differences clustered in the three regions around Glu50, Ile78, and His135 (Figure 7). Inspection of the 3D structure<sup>7,8</sup> revealed that these amino acids cluster all exclusively around the ATP binding cavity (Figure 8). Therefore, binding of **5** to the ATP recognition site was postulated. A similar pattern of shift differences was observed for novobiocin (**3**), known to bind into the ATP pocket, verifying the binding hypothesis of **5**. The final proof was achieved by X-ray structure analysis of the 24 kDa fragment complexed with **5**.<sup>27</sup> Similar patterns of shift differences as for **3** and **5** were observed for many other compounds tested, e.g., **4f**, indicating binding to the ATP site (Table 1). Due to the different structures of the tested compounds, the extent of the induced shifts was of course not always as pronounced as in the case of **5**, even for compounds binding with a similar affinity. As expected, no peak shifts were observed in the case of the quinolone **1**. For some tested ATPase assay hits no binding or even binding to other sites was detected. For example the



**Figure 8.** X-ray structure of **5** complexed to the 24 kDa fragment<sup>27</sup> illustrating shift differences of  $^1\text{H}/^{15}\text{N}$  cross-peaks of protein backbone NHs which are observed by heteronuclear  $^1\text{H}/^{15}\text{N}$  correlation NMR spectroscopy upon addition of **5**. Depicted is the protein backbone of the 24 kDa fragment (white), the indazole **5** (green), the water molecule Wat45 (red), and all protons of the backbone amide NHs which were shifted  $>0.16$  ppm (white balls). The extent of the induced cross-peak shifts is displayed proportionally by the sizes of the Hs, i.e., white balls. The shifted cross-peaks cluster exclusively around the ATP binding pocket. The picture was prepared by MOLOC and WebLab ViewerPro.

catechole **4b** did obviously not bind to the ATP binding site although it exhibited a more potent DNA gyrase inhibitory activity in the supercoiling assay than **4f** or **5** (MNEC = 63  $\mu\text{g}/\text{mL}$ ). Similar to catecholes, no binding to the ATP site could be observed for 2-aminothiazoles, thiophenylamides, and carbamates despite their inhibitory activity in the supercoiling assay.

**X-ray Analysis** was used to verify binding of a compound to the ATP binding site and as a tool to guide the following optimization of these ligands. Instead of the 24 kDa fragment of DNA gyrase subunit B from *S. aureus* used for AUC, SPR, and NMR experiments, a loop deletion mutant of it was used which behaved more favorable during crystallization experiments.<sup>27,28</sup> This mutant was obtained by deletion mutagenesis of residues 97–119 linking directly residues Thr96 and Ser120.

**Figure 9.****Figure 10.** Different needle classes containing identical side chains.

According to X-ray data the loop deletion mutant comprised the ATP recognition site as in the unmodified 24 kDa fragment and as in the published DNA gyrase X-ray structures<sup>7,8</sup> which all describe complexes of *E. coli* DNA gyrase fragments. Unspecific binding of a ligand to a protein can lead to unspecific protein aggregation and, consequently, to protein sedimentation during crystallization experiments. Such unfavorable compounds were identified during AUC experiments and excluded from crystallization trials, raising its success rate. Using this prescreening procedure and the loop deletion mutant protein, numerous X-ray structures were solved for a range of very different ligand structures. Already during the hit validation phase the X-ray structures of the complexes with the indazole **5**, the 2-amino-triazine **4d**, and the pyrrolopyrimidine **6** were determined.<sup>27</sup>

As a consequence of this hit validation process we could focus in the subsequent hit exploration and optimization on phenoles, 2-amino-triazines, 4-amino-pyrimidines, 2-amino-pyrimidines, pyrrolopyrimidines, indazoles, and 2-hydroxymethylindoles (Table 1).

### Ranking of Validated Needles

Although the hit validation process allowed reducing the initial hit list from 14 structural classes to seven, we felt a need to prioritize and rank the validated needle classes. The classical way would be to synthesize and characterize close analogues, i.e., compounds belonging to different needle classes but containing identical side chains, e.g., **7b**<sup>29–31</sup>–**12b** (Figure 10). However, **12b** would hardly be comparable to **7b**–**11b** since the different substituent sites and exit vectors would result in a different overall topology. Comparing just the unsubstituted needles **7a**–**12a** in the ATPase assay or supercoiling assay was not possible, since they were all inactive in these assays (MNEC > 250  $\mu\text{g/mL}$ ). However, the high sensitivity of heteronuclear  $^1\text{H}/^{15}\text{N}$  correlation NMR spectroscopy allowed determining the dissociation constant  $K_D$  of the unsubstituted needles to the 24 kDa

**Table 2.** Dissociation Constants  $K_D$  of Needles Determined by Heteronuclear  $^1\text{H}/^{15}\text{N}$  Correlation NMR Spectroscopy

		$K_D$ [mM]
	<b>12a</b>	10
	<b>7a</b>	60
	<b>9a</b>	60
	<b>8a</b>	200
	<b>10a</b>	200

fragment. The results are summarized in Table 2. Clearly, the highest affinity was observed for **12a**, the lowest for **8a** and **10a**.

With respect to the X-ray data of the ATP binding site,<sup>27</sup> the relative magnitude of the  $K_D$  values could be rationalized by the following considerations. (1) The indazole **12a** fitted much better into the ATP binding cavity whereas the smaller **7a**–**10a** led to voids, giving rise to less favorable van der Waals interactions. (2) The water molecule Wat15 (Figure 3) was most likely displaced by **12a** (as observed in the X-ray structure of **5**), resulting in a favorable entropy contribution. In the case of the smaller compounds **7a**–**10a**, Wat15 was very likely not displaced (as observed in the X-ray structure of **4d**). (3) It was assumed that Wat15 was forming a favorable hydrogen bond with N3 of **7a** or **9a**, respectively (as observed in the X-ray structure of **4d**). For **8a** and **10a** such H-bonds were not possible without breaking the H-bond network to Wat45 and Asp73.

### 3D Guided Optimization Process

The preliminary SARs of the validated needles, the detailed SARs for cyclothialidines<sup>13,14</sup> and coumarins,<sup>32</sup> and—most importantly—the 3D structural knowledge of the active site derived from the X-ray structures of the 24 kDa fragment complexed with ADPNP, **2**, **3**, **5** or **4d** or **6**,<sup>7,8,27</sup> respectively, were employed to guide the optimization of the validated hits. Since the principal considerations for the optimization were identical for all validated needle classes, we will focus in the following on indazoles only.

As a first criteria we postulated that a DNA gyrase inhibitor must not only form a hydrogen bond network with Asp73 and the very firmly bound water molecule Wat45, but it must also contain a side chain stacking on the Glu50-Arg76 salt bridge (Figure 11). This hypothesis allowed the explanation of the improved DNA gyrase inhibitory activity of **4h** compared to **12a** (Table 3). With a second generation of indazoles it was attempted to introduce additional structural elements that were able to form H-bonds to Arg136.<sup>33</sup> This second postulate was realized by compounds such as **13**. The indazole **13** was obtained by conversion of **14**<sup>34</sup> with 4-methyl-7-thiocoumarin followed by treatment with TFA (Scheme 1). In contrast to our expectation, not more than just minor improvements of DNA gyrase



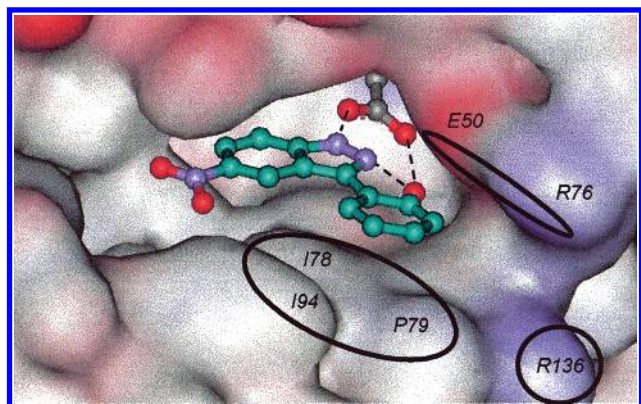


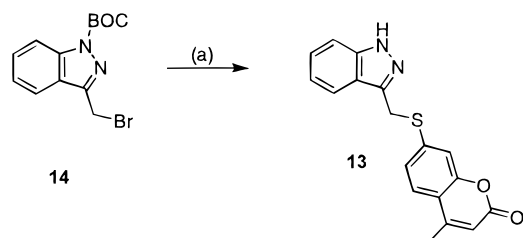
**Figure 11.** Refined binding model: the additional sites of expected, favorable interactions between a ligand and the ATP binding pocket are marked in the X-ray structure of the 24 kDa fragment complexed with **5**. With the exception of the Asp73 side chain the protein is presented by its surface only. Dashed lines: observed H-bonds between inhibitor, protein, and conserved water Wat45. The picture was prepared by MOLOC and WebLab ViewerPro.

**Table 3.** DNA Gyrase Inhibition by Indazoles

		MNEC [ $\mu\text{g/ml}$ ] <sup>1</sup>	
- R <sub>4</sub>	- R <sub>3</sub>		
- H	- H	<b>12a</b>	>250
- H		<b>4h</b>	8
- H		<b>13</b>	8
		<b>22</b>	0.25
		<b>23</b>	0.03
<hr/>			
		<b>3</b>	0.25

<sup>1</sup> MNECs are determined in the supercoiling assay, except for **12a**.

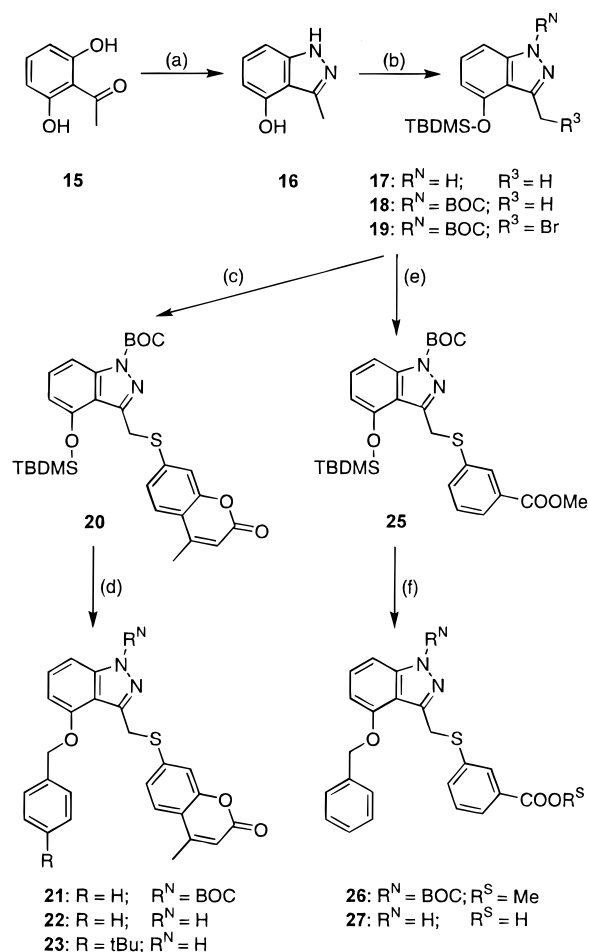
**Scheme 1.** Synthesis of 3-Substituted Indazole **13**<sup>a</sup>



<sup>a</sup> Reagents and conditions: (a) (1) 4-methyl-7-thiocoumarin, Et<sub>3</sub>N, CH<sub>2</sub>Cl<sub>2</sub>, 2 h, rt; (2) TFA, CH<sub>2</sub>Cl<sub>2</sub>, 3 h, rt.

inhibition were observed within this series. To exploit the potential of van der Waals interactions between a ligand and a lipophilic area formed by Ile78, Pro79, and Ile94, a third series of indazoles was prepared contain-

**Scheme 2.** Synthesis of Indazoles **22**, **23** and **27**



<sup>a</sup> Reagents and conditions: (a) N<sub>2</sub>H<sub>4</sub>·H<sub>2</sub>O, HOCH<sub>2</sub>CH<sub>2</sub>OH, 2 h, 160 °C; (b) (1) TBDMSCl, imidazole, DMF, 12 h, rt; (2) (BOC)<sub>2</sub>O, Et<sub>3</sub>N, DMAP, MeCN, 3 h, rt; (3) NBS, (PhCO<sub>2</sub>)<sub>2</sub>, CCl<sub>4</sub>, 4.5 h, 78 °C; (c) 4-methyl-7-thiocoumarin, Et<sub>3</sub>N, CH<sub>2</sub>Cl<sub>2</sub>, 4 h, rt; (d) (1) BnBr or *p*-*t*Bu-BnBr, KF, DMF, 4 h, rt; (2) TFA, CH<sub>2</sub>Cl<sub>2</sub>, 4 h, rt; (e) 3-mercapto-benzoic acid methyl ester (**24**), Et<sub>3</sub>N, CH<sub>2</sub>Cl<sub>2</sub>, 4 h, rt; (f) (1) BnBr, KF, DMF, 2 h, rt; (2) LiOH, THF, MeOH, H<sub>2</sub>O, 5 h, rt.

ing a second side chain. This series of 3,4-disubstituted indazoles was synthesized according to the procedure outlined in Scheme 2. A pronounced improvement of inhibitory activity could be observed for **22**. Optimizing the DNA gyrase inhibitory activity of **22** led to **23** containing an additional *tert*-butyl group. It was about 10 times more active than **3** in the DNA gyrase assay while still being structurally much less complex than **3**. The final proof of our binding hypotheses was achieved by the X-ray structure of **27** complexed to the 24 kDa fragment (Figure 12). In this structure, (1) the indazole scaffold formed the postulated H-bond network with Asp73 and Wat45, (2) the mercapto-benzoic acid side chain stacked on the Glu50-Arg76 salt bridge and was H-bonded to Arg136, and (3) the benzyloxy side chain formed van der Waals interactions with the lipophilic area Ile78-Pro79-Ile94.

## Conclusions

Our novel approach combining (1) an *in silico* needle screen, (2) a biased DNA gyrase needle screen, (3) a hit validation protocol, and (4) a 3D guided optimization process has led to a series of potent, novel inhibitors of

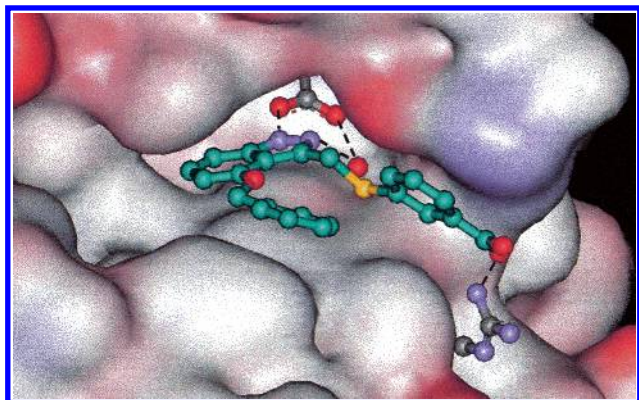


**Figure 12.** X-ray structure of the 24 kDa fragment complexed with **27**. With the exception of the Asp73 and Arg136 side chains, the protein is presented by its surface only. Dashed lines: observed H-bonds between inhibitor, protein, and conserved water Wat45. The picture was prepared by MOLOC and WebLab ViewerPro.

DNA gyrase. Running the *in silico* screening prior to the enzyme assay allowed us to focus early on the most promising candidates in our compound library, increasing the hit rate and being highly time- and cost-efficient. Besides the classical ways of validating screening hits by biological experiments and preliminary SARs, biophysical methods were applied to eliminate rapidly and unambiguously false positives. The high sensitivity of NMR spectroscopy was used to elaborate a ranking of the validated needles with respect to their binding affinities. Such a ranking may have a decisive influence on the prioritization of tasks and on the selection of the most promising needle for the following lead optimization processes. The optimization process itself—converting the screening hits into potent lead structures—was strongly guided by the detailed knowledge of the active site's 3D structure, enabling us to focus the synthetic efforts early on the most promising side chains of the inhibitors. The lead optimization is exemplified by the indazole series resulting in **23**, a 10 times more potent DNA gyrase inhibitor than novobiocin (**3**). Overall, our novel approach represents an attractive alternative to random screening.

## Experimental Section

**DNA Gyrase Assays.** Assay conditions of the ATPase and supercoiling assay were described previously.<sup>22,23</sup> Both assays led to at least similar, if not identical MNECs.

**24 kDa Fragments.** The 24 kDa N-terminal fragments of the DNA gyrase subunit B of *S. aureus* and the corresponding loop deletion mutant were obtained as described previously.<sup>11,28</sup> The 24 kDa fragment used for AUC, SPR, and NMR consisted of the residues 15–223, including the mutation A18V. Except the deleted residues 97–119 the loop deletion mutant used for X-ray analysis consisted of the whole N terminus ending with residue 223.

**Analytical Ultracentrifugation.** Ultracentrifugation experiments were performed at 20 °C on a Beckman Optima XL-A. A run contained up to 21 samples of 100  $\mu$ L volume at a ligand concentration yielding a ligand absorbance of  $\geq 0.1$  OD at a wavelength preferably  $> 280$  nm. Typical ligand concentrations were 100  $\mu$ M. The concentration of the 24 kDa fragment of DNA gyrase B was adapted to the ligand concentration in order to result a 10-fold ligand excess. The buffer contained 75 mM  $\text{NH}_4\text{CO}_3$ , pH 8.6, 0.02%  $\text{NaN}_3$ , 2.5% DMSO. A ligand free sample was centrifuged in each run as a control. Data were analyzed according to DISCREET.<sup>35</sup> Optimal velocity was 18 000 rpm.

## Surface Plasmon Resonance Binding Experiments<sup>36,37</sup>

Surface plasmon resonance studies were performed on a Biacore 2000 instrument. A CM5 sensor chip was used, equipped with a carboxymethyl-dextran-modified gold surface. The 24 kDa fragment of DNA gyrase B was immobilized in three channels of the sensor chip using the fourth channel as a reference. The 24 kDa fragment was immobilized according to the procedure described by Johnsson et al.<sup>38</sup> The protein solution needed for the immobilization procedure was freshly prepared and contained 100  $\mu$ g/mL 24 kDa fragment in 9 mM acetate, 1 mM Hepes buffer at pH 4.9. In a typical immobilization, different amounts of protein were bound on the surfaces of the three flow channels, e.g., 700, 5524, and 7807 pg/mm<sup>2</sup>. The amount of bound protein was controlled via different time intervals of contact. Excess activated carboxyl functions on the dextran layer were quenched after the immobilization by contacting the sensor surface with ethanolamine. The sensor surface was washed shortly (30 s) with an SDS solution (1%) to dissolve protein aggregates on the surface formed during the immobilization. The activity of the immobilized 24 kDa fragment was controlled after the immobilization procedure and between successive binding experiments by contacting the surface with a solution of **3**. The association and dissociation rate constants ( $k_a$ ,  $k_d$ ) and the equilibrium sensor response ( $R_{eq}$ ) were taken as quality criteria. Typical values of  $k_d$  and  $k_a$  for **3** were  $3\text{--}4 \times 10^{-3} \text{ s}^{-1}$  and  $1\text{--}3 \times 10^6 \text{ M}^{-1} \text{ s}^{-1}$ . The equilibrium sensor response depended on the amount of protein immobilized and the concentration of **3** in solution. The binding capacity of the immobilized protein was in the order of 0.1–0.15 depending on the amount of protein immobilized.

During a time interval of 5 min the compounds to be tested were exposed to the sensor surface as 2.5, 25, or 250  $\mu$ M solutions, respectively, in a Hepes buffer (10 mM, pH 7.5, 150 mM NaCl, 3 mM EDTA, 0.005% polysorbate 20 (v/v), 1% DMSO).

Two decisive criteria were used to identify the compounds binding to the 24 kDa fragment: (1) a positive sensor response after the contact interval; (2) a ranking of the sensor responses detected for the different channels that is comparable to the ranking observed for controls, i.e., for **3**. This ranking was interpreted as indication for protein specificity of the binding.

**NMR Spectroscopy for Hit Validation.** A typical two-dimensional  $^1\text{H}$ - $^{15}\text{N}$  correlated NMR sample contained 7 mM of compound to be tested, 0.7 mM 24 kDa fragment of DNA gyrase subunit B, 75 mM  $\text{NH}_4\text{CO}_3$ , 0.02%  $\text{NaN}_3$ , 2.5% DMSO in 90%  $\text{H}_2\text{O}$ , 10%  $\text{D}_2\text{O}$ , pH 8.6. The spectra were recorded at 600 MHz on a Bruker DMX 600 NMR instrument at a temperature of 300 K. Spectral parameters were 512 complex points in F2 at a width of 9615 Hz (proton dimension) and 64 complex points in F1 at a width of 1766 Hz (nitrogen dimension). The radio frequency carriers were set at the water resonance line (4.75 ppm) for  $^1\text{H}$  and at 117.0 ppm for  $^{15}\text{N}$ . Normally 32 scans were acquired for each FID resulting in a total measurement time of 66 min. Data were transferred to a SGI Unix workstation and processed using the NIH software package NMRPipe.<sup>39</sup> Spectral interpretation was performed with the aid of the XEASY<sup>40</sup> program. Herein, the 2D spectrum of a protein–ligand solution was compared to a reference spectrum of the apo-enzyme that contained 2.5% DMSO only, but no ligand. The secondary chemical shifts were calculated from the  $^1\text{H}$  and  $^{15}\text{N}$  shift coordinates of the cross-peaks:  $\{[\Delta\delta(^1\text{H})]^2 + [\Delta\delta(^{15}\text{N})0.3]^2\}^{1/2}$ .

**NMR Spectroscopy for Ranking of Needles.** For each compound the two-dimensional  $^1\text{H}$ - $^{15}\text{N}$  correlated NMR spectrum was recorded at 10 different concentrations ranging from 0 to 22 mM and ligand/protein ratios from 0 to  $\sim 50$ , respectively. The samples were prepared by adding small amounts of a 200 mM ligand stock solution in DMSO to the protein solution containing the  $^{15}\text{N}$  labeled 24 kDa fragment at a concentration of 0.45 mM in 75 mM ammonium phosphate buffer, pH 8.6. To account for shifts induced by DMSO a titration was performed adding just DMSO to the protein solution. The spectra were recorded and processed as described for the hit validation. For the determination of dissociation



constants ( $K_D$ ), nonlinear least-squares fits of shifts versus ligand concentration were performed using the public domain program *xmgr* (version 3.01) according to the equation  $\delta = (A_0X/(X + A_1)) + A_2$ , with  $\delta$  equal to the change in chemical shift ( $^1\text{H}$  or  $^{15}\text{N}$ ),  $X$  = concentration of ligand,  $A_0$  = maximum change in chemical shift,  $A_1 = K_D$ , and  $A_2$  = (chemical shift) offset.

**X-ray.** Experimental details for the crystallization experiments and X-ray analysis were described by Kostrewa et al.<sup>27</sup> and Dale et al.<sup>28</sup>

**Chemistry. General Information.** Compounds **1**, **3**, **4b**, **4e**, **7a**, **8a**, **9a**, **10a**, **12a**, 4-methyl-7-thiocoumarin, and 3-mercaptopbenzoic acid were commercially available. The syntheses of the compounds **2**,<sup>13,14</sup> **4a**,<sup>41</sup> **4f**,<sup>42</sup> **4h**,<sup>43</sup> **5**,<sup>43</sup> **7b**,<sup>30,31</sup> **11a**,<sup>44</sup> **14**,<sup>34</sup> and **16**<sup>45,46</sup> were described already. Unless indicated otherwise, commercially available chemicals and solvents were used without further purification. Silica gel 60 (0.04–0.063 mm; Merck) was used for flash chromatography.  $^1\text{H}$  NMR spectroscopy was performed on a Bruker 250 MHz or 400 MHz machine using the indicated solvent with TMS as internal standard. Chemical shifts  $\delta$  are given in ppm relative to TMS, coupling constants  $J$  in Hz.

**7-(1*H*-Indazole-3-ylmethylsulfanyl)-4-methylcoumarin (13).** To a solution of **14** (90 mg, 0.29 mmol) and 4-methyl-7-thiocoumarin (61 mg, 0.32 mmol) in  $\text{CH}_2\text{Cl}_2$  (3 mL) was added  $\text{Et}_3\text{N}$  (44  $\mu\text{L}$ , 0.32 mmol). After the mixture was stirred for 2 h at room temperature,  $\text{H}_2\text{O}$  (10 mL) was added and the mixture was extracted with EtOAc. The organic layer was washed with brine and dried ( $\text{Na}_2\text{SO}_4$ ) before the solvent was evaporated. The obtained oil was dissolved in  $\text{CH}_2\text{Cl}_2$  (4 mL), and TFA (0.3 mL) was added. After 3 h at room temperature the reaction mixture was neutralized with saturated  $\text{NaHCO}_3$  solution and extracted with EtOAc. The organic layer was once again washed with brine and dried ( $\text{Na}_2\text{SO}_4$ ), and the solvent was evaporated. The residue was precipitated from  $\text{CHCl}_3$  and hexane, providing **13** (71 mg, 76%) as a white powder.  $^1\text{H}$  NMR (DMSO- $d_6$ ):  $\delta$  12.94 (1H, s), 7.89 (1H, d,  $J = 7.8$ ), 7.63 (1H, d,  $J = 7.8$ ), 7.55–7.45 (2H, m), 7.39–7.30 (2H, m), 7.12 (1H, t,  $J = 7.8$ ), 6.31 (1H, s), 4.75 (2H, s), 2.38 (3H, s). MS (EI+):  $m/z$  322 ( $\text{M}^+$ ). HRMS calcd for  $\text{C}_{18}\text{H}_{14}\text{N}_2\text{O}_2\text{S}$  322.0776, found 322.0773.

**3-Methyl-1*H*-indazol-4-ol (16).** A solution of 2,6-dihydroxyacetophenone (**15**; 50 g, 331 mmol) in ethyleneglycol (750 mL) was added dropwise to a solution of hydrazine hydrate (33 g, 659 mmol) in ethyleneglycol (250 mL). The reaction mixture was stirred for 20 min at room temperature, then heated to 160  $^\circ\text{C}$  for 2 h. The solution was allowed to cool to room temperature, and it was poured into  $\text{H}_2\text{O}$  (2L). The pH was adjusted to pH 6 by adding AcOH (25 mL), and the mixture was extracted with EtOAc (4  $\times$  1L). The combined organic layers were washed with 5%  $\text{Na}_2\text{SO}_3$ , dried ( $\text{Na}_2\text{SO}_4$ ), and concentrated. Chromatography (toluene/acetonitrile 7:3) provided **16** (36.7 g, 68%) as a white solid.  $^1\text{H}$  NMR (DMSO- $d_6$ ):  $\delta$  12.34 (1H, s, br), 9.89 (1H, s), 7.03 (1H, t,  $J = 7.8$ ), 6.80 (1H, d,  $J = 7.8$ ), 6.32 (1H, d,  $J = 7.8$ ), 2.55 (3H, s). MS (EI+):  $m/z$  148 ( $\text{M}^+$ ).

**4-(*tert*-Butyl-dimethyl-silanyloxy)-3-methyl-1*H*-indazole (17).** Imidazole (3.08 g, 45.20 mmol) and *tert*-butyldimethylchlorosilane (1.57 g, 10.40 mmol) were added to a cooled solution (0  $^\circ\text{C}$ ) of **16** (1.34 g, 9.04 mmol) in DMF (100 mL). The solution was stirred for 12 h at room temperature. Then  $\text{H}_2\text{O}$  (100 mL) was added, and the mixture was extracted with EtOAc (3  $\times$  50 mL). The organic extracts were washed with  $\text{H}_2\text{O}$  and brine and dried ( $\text{Na}_2\text{SO}_4$ ). Evaporation of the solvent and chromatography (hexane/EtOAc 2:1 to 1:1) provided **17** (2.10 g, 89%) as a white solid.  $^1\text{H}$  NMR (DMSO- $d_6$ ):  $\delta$  12.5 (1H, s, br), 7.12 (1H, t,  $J = 7.8$ ), 6.98 (1H, d,  $J = 7.8$ ), 6.39 (1H, d,  $J = 7.8$ ), 2.57 (3H, s), 1.01 (9H, s), 0.31 (6H, s). MS (EI+):  $m/z$  262 ( $\text{M}^+$ ).

**4-(*tert*-Butyl-dimethyl-silanyloxy)-3-methyl-indazole-1-carboxylic Acid *tert*-Butyl Ester (18).** DMAP (43 mg, 0.35 mmol) was added to a solution of **17** (462 mg, 1.76 mmol) and  $\text{Et}_3\text{N}$  (270  $\mu\text{L}$ , 1.94 mmol) in acetonitrile (3 mL). The mixture was cooled to 0  $^\circ\text{C}$ , and a solution of (BOC) $_2\text{O}$  (461 mg, 2.11

mmol) in acetonitrile (3 mL) was added dropwise. The solution was allowed to warm to room temperature stirred for 3 h. Evaporation of the solvent and chromatography (hexane/EtOAc 4:1) provided **18** (468 mg, 73%) as an oil.  $^1\text{H}$  NMR (DMSO- $d_6$ ):  $\delta$  7.63 (1H, d,  $J = 7.8$ ), 7.41 (1H, t,  $J = 7.8$ ), 6.75 (1H, d,  $J = 7.8$ ), 2.59 (3H, s), 1.62 (9H, s), 1.01 (9H, s), 0.34 (6H, s). MS (EI+):  $m/z$  362 ( $\text{M}^+$ ).

**3-Bromomethyl-4-(*tert*-butyl-dimethyl-silanyloxy)-indazole-1-carboxylic Acid *tert*-Butyl Ester (19).** To a solution of **18** (440 mg, 1.21 mmol) in  $\text{CCl}_4$  (5 mL) heated to reflux was added a mixture of *N*-bromosuccinimide (215 mg, 1.21 mmol) and benzoylperoxide (29 mL, 0.12 mmol) in small portions. The mixture was refluxed for another 4.5 h, then cooled to room temperature, and filtered. After evaporation of the solvent and chromatography (hexane/EtOAc 15:1), **19** was obtained as an oil (385 mg, 72%).  $^1\text{H}$  NMR (DMSO- $d_6$ ):  $\delta$  7.71 (1H, d,  $J = 8.0$ ), 7.53 (1H, t,  $J = 8.0$ ), 6.87 (1H, d,  $J = 8.0$ ), 4.97 (2H, s), 1.68 (9H, s), 1.08 (9H, s), 0.42 (6H, s). MS (EI+):  $m/z$  440 ( $\text{M}^+$ ).

**4-(*tert*-Butyl-dimethyl-silanyloxy)-3-(4-methylcoumarin-7-ylsulfanylmethyl)-indazole-1-carboxylic Acid *tert*-Butyl Ester (20).** A solution of **19** (380 mg, 0.86 mmol) and 4-methyl-7-thiocoumarin (182 mg, 0.95 mmol) in  $\text{CH}_2\text{Cl}_2$  (5 mL) containing  $\text{Et}_3\text{N}$  (132  $\mu\text{L}$ , 0.95 mmol) was stirred 4 h at room temperature.  $\text{H}_2\text{O}$  (10 mL) was added, and the mixture was extracted with EtOAc. The organic extracts were washed with brine, dried ( $\text{Na}_2\text{SO}_4$ ), and concentrated. Chromatography (hexane/EtOAc 1:1) provided **20** (428 mg, 90%) as a white solid.  $^1\text{H}$  NMR (DMSO- $d_6$ ):  $\delta$  7.66 (1H, d,  $J = 8.0$ ), 7.64 (1H, d,  $J = 8.0$ ), 7.54 (1H, d,  $J = 1.5$ ), 7.47 (1H, t,  $J = 8.0$ ), 7.31 (1H, dd,  $J_1 = 8.0$ ,  $J_2 = 1.5$ ), 6.81 (1H, d,  $J = 8.0$ ), 6.33 (1H, s), 4.71 (2H, s), 2.40 (3H, s), 1.60 (9H, s), 0.97 (9H, s), 0.35 (6H, s). MS (EI+):  $m/z$  552 ( $\text{M}^+$ ).

**4-Benzoyloxy-3-(4-methylcoumarin-7-ylsulfanylmethyl)-indazole-1-carboxylic Acid *tert*-Butyl Ester (21).** KF (42 mg, 0.72 mmol) was added to a suspension of **20** (200 mg, 0.36 mmol) and benzyl bromide (52  $\mu\text{L}$ , 0.43 mmol) in DMF (10 mL). After the mixture was stirred for 4 h at room temperature,  $\text{H}_2\text{O}$  (20 mL) was added and the mixture was extracted with EtOAc. The combined organic layers were washed with brine and dried ( $\text{Na}_2\text{SO}_4$ ), and the solvent was evaporated. The residue was precipitated from  $\text{CHCl}_3$  and hexane yielding **21** (153 mg, 80%) as a white solid.  $^1\text{H}$  NMR (DMSO- $d_6$ ):  $\delta$  7.67–7.46 (7H, m), 7.33–7.26 (3H, m), 6.99 (1H, d,  $J = 8.0$ ), 6.34 (1H, s), 5.30 (2H, s), 4.68 (2H, s), 2.41 (3H, s), 1.62 (9H, s).

**7-(4-Benzoyloxy-1*H*-indazol-3-ylmethylsulfanyl)-4-methylcoumarin (22).** A solution of **21** (151 mg, 0.29 mmol) in  $\text{CH}_2\text{Cl}_2$  (4 mL) containing TFA (0.5 mL) was stirred for 4 h at room temperature. The reaction mixture was neutralized with saturated  $\text{NaHCO}_3$  solution and extracted with EtOAc. The organic layer was washed with brine and dried ( $\text{Na}_2\text{SO}_4$ ), and the solvent was evaporated. The residue was precipitated from  $\text{CHCl}_3$  and hexane, providing **22** (112 mg, 91%) as white powder.  $^1\text{H}$  NMR (DMSO- $d_6$ ):  $\delta$  12.96 (1H, s), 7.66 (1H, d,  $J = 8.0$ ), 7.60–7.49 (3H, m), 7.36–7.24 (5H, m), 7.07 (1H, t,  $J = 8.0$ ), 6.67 (1H, t,  $J = 8.0$ ), 6.35 (1H, s), 5.28 (2H, s), 4.72 (2H, s), 2.43 (3H, s). MS (EI+):  $m/z$  428 ( $\text{M}^+$ ). HRMS calcd for  $\text{C}_{25}\text{H}_{20}\text{N}_2\text{O}_5\text{S}$  428.1195, found 428.1194.

**7-[4-(4-*tert*-Butyl-benzoyloxy)-1*H*-indazol-3-ylmethylsulfanyl]-4-methylcoumarin (23).** KF (42 mg, 0.72 mmol) was added to a suspension of **20** (200 mg, 0.36 mmol) and 4-*tert*-butylbenzyl bromide (80  $\mu\text{L}$ , 0.43 mmol) in DMF (10 mL). After being stirred for 4 h at room temperature,  $\text{H}_2\text{O}$  (20 mL) was added and the mixture was extracted with EtOAc. The combined organic layers were washed with brine and dried ( $\text{Na}_2\text{SO}_4$ ), and the solvent was evaporated. The residue was dissolved in  $\text{CH}_2\text{Cl}_2$  (5 mL), and TFA (1 mL) was added. After 3 h at room temperature the reaction mixture was neutralized with saturated  $\text{NaHCO}_3$  solution and extracted with EtOAc. The organic layer was once again washed with brine and dried ( $\text{Na}_2\text{SO}_4$ ), and the solvent was evaporated. The residue was precipitated from  $\text{CHCl}_3$  and hexane, providing **23** (158 mg, 90%) as a gray powder.  $^1\text{H}$  NMR (DMSO- $d_6$ ):  $\delta$  12.98 (1H, s, br), 7.69 (1H, d,  $J = 8.0$ ), 7.50 (1H, d,  $J = 1.2$ ), 7.40 (2H, d,  $J$

= 9.0), 7.34 (1H, t,  $J_1 = 8.0$ ,  $J_2 = 1.2$ ), 7.28 (1H, t,  $J = 8.0$ ), 7.13 (2H, d,  $J = 9.0$ ), 7.06 (1H, d,  $J = 8.0$ ), 6.65 (1H, d,  $J = 8.0$ ), 6.34 (1H, s), 5.20 (2H, s), 4.73 (2H, s), 2.42 (3H, s), 1.16 (9H, s). MS (ISP):  $m/z$  485 ( $(M + H)^+$ ). HRMS calcd for  $C_{29}H_{28}N_2O_3S$  484.1821, found 484.1823.

**3-Mercapto-benzoic Acid Methyl Ester (24).** A solution of 3-mercapto-benzoic acid (1.00 g, 6.48 mmol) in 4 M methanolic HCl was refluxed 4 h. After evaporation, the residue was dissolved in ethyl acetate and extracted with  $NaHCO_3$ . The organic layer was washed with brine, dried ( $MgSO_4$ ), and concentrated to dryness yielding **24** as a dark yellow oil (1.09 g, quant.).  $^1H$  NMR ( $DMSO-d_6$ ):  $\delta$  7.91 (1H, s), 7.70 (1H, d,  $J = 7.6$ ), 7.56 (1H, d,  $J = 7.8$ ), 7.40 (1H, t,  $J = 7.7$ ), 5.88 (1H, s), 3.85 (3H, s). MS (EI+):  $m/z$  168 ( $M^+$ ).

**4-(tert-Butyl-dimethyl-silanyloxy)-3-(3-methoxycarbonyl-phenylsulfanylmethyl)-indazole-1-carboxylic Acid tert-Butyl Ester (25).** A solution of **19** (3.50 g, 7.92 mmol) and **24** (1.40 g, 8.32 mmol) in  $CH_2Cl_2$  (25 mL) containing  $Et_3N$  (1.16 mL, 8.32 mmol) was stirred for 4 h at room temperature. The mixture was diluted with  $CH_2Cl_2$  and washed with brine. The dried ( $MgSO_4$ ) and evaporated organic layer was flash chromatographed (hexane/ $EtOAc$  7:3), providing **25** as a slightly yellow oil (3.72 g, 89%).  $^1H$  NMR ( $CDCl_3$ ):  $\delta$  8.01 (1H, s), 7.86 (1H, d,  $J = 7.0$ ), 7.71–7.64 (2H, m), 7.39–7.30 (2H, m), 6.66 (1H, d,  $J = 7.9$ ), 4.57 (2H, s), 3.90 (3H, s), 1.67 (9H, s), 1.03 (9H, s), 0.37 (6H, s). MS (ISP):  $m/z$  529.3 ( $(M+H)^+$ ).

**4-Benzoyloxy-3-(3-methoxycarbonyl-phenylsulfanylmethyl)-indazole-1-carboxylic Acid tert-Butyl Ester (26).** To a solution of **25** (1.29 g, 2.44 mmol) and benzyl bromide (350  $\mu$ L, 2.93 mmol) in DMF (20 mL) was added KF (283 mg, 4.88 mmol). After the mixture was stirred for 2 h at room temperature,  $H_2O$  (80 mL) was added. The mixture was extracted with  $EtOAc$ . Flash chromatography (hexane/ $EtOAc$  4:1) provided **26** (765 mg, 62%) as a white foam.  $^1H$  NMR ( $DMSO-d_6$ ):  $\delta$  7.82 (1H, s), 7.78 (1H, d,  $J = 7.8$ ), 7.63 (1H, d,  $J = 7.9$ ), 7.61 (1H, s), 7.56–7.21 (4H, m), 7.35–7.28 (3H, m), 6.98 (1H, d,  $J = 8.3$ ), 5.29 (2H, s), 4.58 (2H, s), 3.82 (3H, s), 1.60 (9H, s). MS (EI+):  $m/z$  504 ( $M^+$ ).

**3-(4-Benzoyloxy-1H-indazol-3-ylmethylsulfanyl)-benzoic Acid (27).** To a solution of **26** (757 mg, 1.49 mmol) in THF/ $MeOH/H_2O$  2:1:1 (20 mL) was added  $LiOH \cdot H_2O$  (189 mg, 4.50 mmol). After 5 h at room temperature,  $H_2O$  (50 mL) was added. The pH was adjusted to pH 2 by adding 3 M HCl. The obtained suspension was extracted with  $EtOAc$ . The combined organic layers were dried ( $MgSO_4$ ) and concentrated to dryness. The residue was precipitated from ether and hexane, providing **27** (487 mg, 84%) as a white powder.  $^1H$  NMR ( $DMSO-d_6$ ):  $\delta$  13.1 (1H, s br), 12.9 (1H, s, br), 7.90 (1H, s), 7.74 (1H, d,  $J = 7.5$ ), 7.61 (1H, d,  $J = 7.7$ ), 7.56–7.47 (2H, m), 7.41 (1H, t,  $J = 8.3$ ), 7.33–7.21 (4H, m), 7.03 (1H, d,  $J = 8.4$ ), 6.68 (1H, d,  $J = 7.7$ ), 5.24 (2H, s), 4.62 (2H, s). HRMS calcd for  $C_{22}H_{18}N_2O_3S$  390.1038, found 390.1038. Anal. ( $C_{22}H_{17.5}Li_{0.5}N_2O_3S$ ) C, H, Li, N, S.

**Acknowledgment.** We sincerely thank J.-C. Alt (chemistry), A. D'Arcy (X-ray), A. Arnet (chemistry), G. Dale (X-ray), B. Gsell (NMR), J. Kohler (SPR), K. Kuratli (biology), E. Kusznir (AUC), T. Masquelin (chemistry), F. Montavon (chemistry), W. Pirson (biology), A. Ross (NMR), P. Schmitz (chemistry), H. Senn (NMR), U. Steiert (biology), M. Stihle (X-ray), B. Takacs (biology), and D. Wechsler (chemistry) for their excellent and dedicated work.

## References

- Reece, R. J.; Maxwell, A. DNA Gyrase: Structure and Function. *CRC Crit. Rev. Biochem. Mol. Biol.* **1991**, *26*, 335–375.
- Maxwell, A. The interaction between coumarin drugs and DNA gyrase. *Mol. Microbiol.* **1993**, *9*, 681–686.
- Ho, P.-L.; Que, T.-L.; Tsang, D. N.-C.; Ng, T.-K.; Chow, K.-H.; Seto, W.-H. Emergence of Fluoroquinolone Resistance among Multiply Resistant Strains of *Streptococcus pneumoniae* in Hong Kong. *Antimicrob. Agents Chemother.* **1999**, *43*, 1310–1313.
- Voss, A.; Milatovic, D.; Wallrauch-Schwarz, C.; Rosdahl, V. T.; Braveny, I. Methicillin-Resistant *Staphylococcus aureus* in Europe. *Eur. J. Clin. Microbiol. Infect. Dis.* **1994**, *13*, 50–55.
- Wolfson, J. S. Quinolone Antimicrobial Agents: Adverse Effects and Bacterial Resistance. *Eur. J. Clin. Microbiol. Infect. Dis.* **1989**, *8*, 1080–1092.
- Nakada, N.; Shimada, H.; Hirata, T.; Aoki, Y.; Kamiyama, T.; Watanabe, J.; Arisawa, M. Biological characterization of cyclothialidine, a new DNA gyrase inhibitor. *Antimicrob. Agents Chemother.* **1993**, *37*, 2656–2661.
- Lewis, R. J.; Singh, O. M. P.; Smith, C. V.; Skarzynski, T.; Maxwell, A.; Wonacott, A. J.; Wigley, D. B. The nature of inhibition of DNA gyrase by the coumarins and the cyclothialidines revealed by X-ray crystallography. *EMBO J.* **1996**, *15*, 1412–1420.
- Wigley, D. B.; Davies, G. J.; Dodson, E. J.; Maxwell, A.; Dodson, G. Crystal structure of an N-terminal fragment of the DNA gyrase B protein. *Nature* **1991**, *351*, 624–629.
- Kim, O. K.; Ohemeng, K., A. Patents on DNA Gyrase inhibitors: January 1995 to March 1998. *Exp. Opin. Ther. Patents* **1998**, *8*, 959–969.
- Lambert, H. P.; O'Grady, F. W. Antibiotic and Chemotherapy. In *Coumarins*, 6th ed.; Lambert, H. P., O'Grady, F. W., Eds.; Churchill Livingstone: Edinburgh, 1992; pp 140–141.
- Stieger, M.; Angehrn, P.; Wohlgensinger, B.; Gmuender, H. GyrB mutations in *Staphylococcus aureus* strains resistant to cyclothialidine, coumermycin, and novobiocin. *Antimicrob. Agents Chemother.* **1996**, *40*, 1060–1062.
- Angehrn, P.; Götschi, E. Glucuronidation of Cyclothialidines. Unpublished results.
- Goetschi, E.; Angehrn, P.; Gmuender, H.; Hebeisen, P.; Link, H.; Masciadri, R.; Nielsen, J. Cyclothialidine and its congeners: a new class of DNA gyrase inhibitors. *Pharmacol. Ther.* **1993**, *60*, 367–380.
- Goetschi, E.; Angehrn, P.; Gmuender, H.; Hebeisen, P.; Link, H.; Masciadri, R.; Nielsen, J.; Reindl, P.; Ricklin, F. The DNA gyrase inhibitor cyclothialidine: progenitor of a new class of antibacterial agents. In *Med. Chem.: Today Tomorrow, Proc. AFMC Int. Med. Chem. Symp. - Tokyo, September 1995*; Yamazaki, M., Blackwell Science Ltd.: Oxford, U.K., 1997; pp 263–270.
- For all described DNA gyrase proteins and protein fragments we refer to the *E. coli* numbering scheme.
- Boehm, H. J. The computer program LUDI: a new method for the de novo design of enzyme inhibitors. *J. Comput.-Aided Mol. Des.* **1992**, *6*, 61–78.
- Boehm, H.-J. On the use of LUDI to search the Fine Chemicals Directory for ligands of proteins of known three-dimensional structure. *J. Comput.-Aided Mol. Des.* **1994**, *8*, 623–632.
- Sprague, P. Automated chemical hypothesis generation and database searching with Catalyst. *Perspect. Drug Discovery Des.* **1995**, *3*, 1–20.
- Gasteiger, J.; Rudolph, C.; Sadowski, J. Automatic generation of 3D atomic coordinates for organic molecules. *Tetrahedron Comput. Methodol.* **1990**, *3*, 537–547.
- Gerber, P. R.; Mueller, K. MAB, a generally applicable molecular force field for structure modeling in medicinal chemistry. *J. Comput.-Aided Mol. Des.* **1995**, *9*, 251–268.
- Daylight Chemical Information Systems Inc., Santa Fe, NM.
- Gmuender, H.; Kuratli, K.; Keck, W. Effect of pyrimido[1,6-*a*]benzimidazoles, quinolones, and  $Ca^{2+}$  on the DNA gyrase-mediated cleavage reaction. *Antimicrob. Agents Chemother.* **1995**, *39*, 163–169.
- Nakada, N.; Gmuender, H.; Hirata, T.; Arisawa, M. Characterization of the binding site for cyclothialidine on the B subunit of DNA gyrase. *J. Biol. Chem.* **1995**, *270*, 14286–14291.
- Dwek, R. A. Monographs on Physical Biochemistry: Nuclear Magnetic Resonance (NMR) in the Biochemistry. Applications to enzyme systems. Oxford University Press: New York, 1973; p 396.
- Shuker, S. B.; Hajduk, P. J.; Meadows, R. P.; Fesik, S. W. Discovering high-affinity ligands for proteins: SAR by NMR. *Science* **1996**, *274*, 1531–1534.
- Klaus, W. Peak assignment in the heteronuclear  $^1H/^{15}N$  correlated NMR of the N-terminal 24 kDa fragment of DNA gyrase subunit B of *S. aureus*. Unpublished results.
- Kostrewa, D.; D'Arcy, A. Novel inhibitors of DNA gyrase: X-ray structures. Unpublished results.
- Dale, G. E.; Kostrewa, D.; Gsell, B.; Stieger, M.; D'Arcy, A. Crystal engineering: deletion mutagenesis of the 24kDa fragment of the DNA gyrase B subunit from *Staphylococcus aureus*. *Acta Crystallogr., Sect. D: Biol. Crystallogr.* **1999**, *D55*, 1626–1629.
- The triazine **7b** was presented by Zeneca as a highly potent DNA gyrase inhibitor soon after we succeeded validating triazines.
- Block, M. H. In Search Of New Gyrase Mediated Antibacterial Agents. Cambridge, U.K., September, 1997.

- (31) Poyser, J. P.; Telford, B.; Timms, D.; Block, M. H.; Hales, N. J. Preparation of aminotriazine derivatives as antibacterials. *PCT Int. Appl.* 1999, 59 pp.
- (32) Reusser, F.; Dolak, L. A. Novenamine is the active moiety in novobiocin. *J. Antibiot.* **1986**, 39, 272–274.
- (33) It was known that the mutation Arg136Ile could be induced rapidly by novobiocin, leading to a highly novobiocin resistant *S. aureus* strain. Nevertheless, a primary importance was assigned to a H-bond between an inhibitor and Arg136, since the same mutation did not occur or led to minor resistance in the case of other inhibitors.<sup>11,29</sup>
- (34) Henke, B. R.; Aquino, C. J.; Birkemo, L. S.; Croom, D. K.; Dougherty, R. W., Jr.; Ervin, G. N.; Grizzle, M. K.; Hirst, G. C.; James, M. K.; Johnson, M. F.; Queen, K. L.; Sherrill, R. G.; Sugg, E. E.; Suh, E. M.; Szewczyk, J. W.; Unwalla, R. J.; Yingling, J.; Willson, T. M. Optimization of 3-(1*H*-Indazol-3-ylmethyl)-1,5-benzodiazepines as Potent, Orally Active CCK-A Agonists. *J. Med. Chem.* **1997**, 40, 2706–2725.
- (35) Schuck, P. Simultaneous radial and wavelength analysis with the Optima XL-A analytical ultracentrifuge. *Prog. Colloid Polym. Sci.* **1994**, 94, 1–13.
- (36) Karlsson, R.; Michaelsson, A.; Mattsson, L. Kinetic analysis of monoclonal antibody–antigen interactions with a new biosensor based analytical system. *J. Immunol. Methods* **1991**, 145, 229–240.
- (37) Kumar, S.; Gunnarsson, K. Small molecule drug screening based on surface plasmon resonance. In *Adv. Drug Discovery Tech*; Harvey, A. L., Ed.; Wiley: Chichester, U.K., 1998; pp 97–114.
- (38) Johnsson, B.; Loefaas, S.; Lindquist, G. Immobilization of proteins to a carboxymethyl-dextran-modified gold surface for biospecific interaction analysis in surface plasmon resonance sensors. *Anal. Biochem.* **1991**, 198, 268–277.
- (39) Delaglio, F.; Grzesiek, S.; Vuister, G. W.; Zhu, G.; Pfeifer, J.; Bax, A. NMRPipe: a multidimensional spectral processing system based on UNIX pipes. *J. Biomol. NMR* **1995**, 6, 227–293.
- (40) Bartels, C.; Xia, T.-h.; Billeter, M.; Guentert, P.; Wuethrich, K. The program XEASY for computer-supported NMR spectral analysis of biological macromolecules. *J. Biomol. NMR* **1995**, 6, 1–10.
- (41) Kubota, K.; Funatsu, M.; Kanzawa, K.; Ishikawa, A.; Takeuchi, M. Preparation of aniline derivatives as calcium release-activated calcium channel inhibitors and their uses. *Jpn. Kokai Tokkyo Koho* **1999**, JP 98–10147, 9 pp.
- (42) Traxler, P. M.; Furet, P.; Mett, H.; Buchdunger, E.; Meyer, T.; Lydon, N. 4-(Phenylamino)pyrrolopyrimidines: Potent and Selective, ATP Site directed Inhibitors of the EGF–Receptor Protein Tyrosine Kinase. *J. Med. Chem.* **1996**, 39, 2285–2292.
- (43) Borsche, W.; Scriba, W. Zur Kenntnis der Benzisoxazole. (About Benzisoxazoles.) *Justus Liebigs Ann. Chem.* **1939**, 540, 83–98.
- (44) Crooks, P. A.; Robinson, B. Azaindoles. I. Syntheses of 5-aza- and 5,7-diazaindoles by the noncatalytic thermal indolization of 4-pyridyl- and 4-pyrimidylhydrazones, respectively. *Can. J. Chem.* **1969**, 47, 2061–2067.
- (45) Zhong, Z.; Xu, T.; Chen, X.; Qui, Y.; Zhang, Z.; Hu, H. A new and facile synthesis of 1*H*-indazoles. *J. Chem. Soc., Perkin Trans. 1* **1993**, 1279–1280.
- (46) The herein described synthesis of **16** was easier to perform and gave a much better yield than the method described by Zhong et al.<sup>45</sup>

JM000017S